SUPPLEMENTAL INFORMATION

Supplemental Methods

fMRI acquisition

Both sites acquired 32 axial slices with 3.5mm thickness using an echo-planar gradient-echo T2-weighted pulse sequence (repetition time, 2000ms; echo time, 29 ms; flip angle, 90 degrees; slice spacing, 0; field of view, 20cm; matrix size, 64x64). A high-resolution T1-weighted structural scan was acquired as a three-dimensional MPRAGE in the sagittal plane with the following parameters: inversion time = 450 ms, TR = 8.21 ms, TE = 3.22 ms, flip angle = 15°, field of view = 24 cm, 184 slices, matrix =256x256, acquired resolution = 0.9375 x 0.9375 x 1.0 mm.

Information regarding data harmonization across sites and quality assurance can be found in a previous manuscript [34]. Briefly, our efforts involved assessing image quality and signal to noise ratio (SNR) at each site, and acquiring the same sequences on several non-study control participants who traveled to both sites. We found that resting-state scans had more ventral prefrontal and temporal lobe susceptibility artifact at Stanford than at NYU, and that the slice-based SNR was higher at NYU than at Stanford. Any differences in fMRI acquisition between the two sites were accounted for by using a site variable that was regressed out of the functional connectivity data prior to the statistical analysis. In addition, there was no effect of scanning site when added as a predictor to the GLMs reported in Figs. 1 and 2.

fMRI preprocessing

After dropping the first 5 acquired volumes (10 seconds), the data were motion-corrected using FSL's mcFLIRT (http://fsl.fmrib.ox.ac.uk/fsl/fslwiki/MCFLIRT) and registered to standard space using FSL's FNIRT. The mean white matter (WM) and cerebral spinal fluid (CSF) signal was estimated from the time-series using an MNI-defined WM/CSF mask transformed to the native functional space. The functional time series was residualized with respect to the estimated WM/CSF signal as well as six motion parameters. The data were then spatially smoothed with

full-width half-maximum (FWHM) Gaussian of 6mm, and time points with framewise-displacement of >0.5 mm were scrubbed from the data. Lastly, a bandpass filter was applied to data using cut-off frequencies of 0.008Hz – 0.1Hz. Only subjects with maximum root mean square motion <2mm and fewer than 20 scrubbed volumes were included in analyses. The resulting NIFTIs were transformed to the MNI standard space for downstream analysis.

fMRI parcel-level time series extraction

We parcellated the brain into 133 parcels based on a published cortical parcellation into 100 parcels derived from an independent resting-state fMRI cohort [42], combined with 33 subcortical parcels that included 14 cerebellar parcels [48], 13 striatal parcels [49], right and left amygdala, right and left hippocampus [50] and right and left thalamus [51]. The mean time series for each parcel was estimated by calculating a weighted average of the BOLD signals of all voxels in a parcel, using equation S1 below. To improve signal quality, only voxels for which the signal to noise ratio (SNR) was higher than 100 were used, as suggested in [69]. SNR was estimated by dividing the mean BOLD across time with its standard deviation. Next, parcel-level BOLD signals were centered and scaled using the z-scoring procedure described in [70].

Equation S1: Weighted average BOLD signal $Aw = \left(\frac{\sum_{i=1}^{n} Vi*Wi}{\sum_{i=1}^{n} Wi}\right)$

Where Vi is the BOLD signal of voxel i, and Wi is the weight of the i-th voxel, which was defined as the maximum of 0 and the Pearson correlation coefficient between Vi and the unweighted average BOLD signal across all the voxels in the parcel.

TMS-EEG acquisition

Each of the target sites were stimulated with 60 pulses (biphasic TMS pulses, 120% of resting motor threshold), interleaved at a random interval of 3 ± 0.3 seconds using a MCF-B65 butterfly coil and a MagPro R30 TMS stimulator (MagVenture, Denmark). 64-channel EEG data were recorded using two 32-channel TMS-compatible BrainAmp DC amplifiers and the Easy EEG cap

with extra flat, freely rotatable electrodes designed specifically for TMS applications (BrainProducts GmbH, Germany). Electrode impedances were kept below 5 kOhms. EEG data were sampled at 5 kHz and an electrode attached to the tip of the nose was used as the reference. The electrodes were digitized relative to the scalp at the end of the TMS-EEG session using the neuronavigation system. To avoid the artifact introduced by the coil recharge, the recharge time was delayed by 1500 ms.

TMS-EEG preprocessing

Preprocessing was accomplished through an automated artifact rejection algorithm described previously [71]. Source localization was performed using the minimum-norm estimation approach [72] to convert the channel-space EEG into the source-space signals of 3003 vertices. Specifically, a three-layer (scalp, skull, and cortical surface) boundary element head model was computed with the OpenMEEG plugin [73] based on FreeSurfer average brain template [74]. A total of 3003 dipoles with unconstrained orientations were generated. The lead-field matrix relating the dipole activities to the EEG was obtained as a result of the boundary element modeling. Given channel-space EEG signals $\mathbf{Z} \in \mathbb{R}^{M\times T}$ of M channels and T sampling points and the lead-field matrix $\mathbf{L} \in \mathbb{R}^{M\times 9009}$, the source signals $\mathbf{X} \in \mathbb{R}^{9009\times T}$ could be estimated via

$$\mathbf{X} = \mathbf{A}\mathbf{Z}$$

where $\mathbf{A} = \mathbf{R}\mathbf{L}^{\mathrm{T}}(\mathbf{L}\mathbf{R}\mathbf{L}^{\mathrm{T}} + \lambda\boldsymbol{\Gamma})^{-1} \in \mathbb{R}^{9009\times M}$ is the inverse operator derived from the minimum-norm estimation. $\mathbf{R} \in \mathbb{R}^{9009\times 9009}$ is the source covariance matrix encoding depth weights to compensate for the bias of assigning larger source estimates towards superficial locations, $\boldsymbol{\Gamma} \in \mathbb{R}^{M\times M}$ the noise covariance matrix, and λ the regularization parameter. Following recommendations in the literature[75], $\mathbf{R} = \mathrm{diag}(r_i)$ with $r_i = (\|\mathbf{L}_{i,1}\|_2^2 + \|\mathbf{L}_{i,2}\|_2^2 + \|\mathbf{L}_{i,3}\|_2^2)^{-1/2}$, where $\mathbf{L}_{i,k}(k = 1, 2, 3)$ are the three columns of $\mathbf{L}$ associated with the i-th vertex, $\lambda = \frac{\delta\cdot\mathrm{trace}(\tilde{\mathbf{L}}\tilde{\mathbf{L}}^{\mathrm{T}})}{M}$, where $\tilde{\mathbf{L}} = \boldsymbol{\Gamma}^{-1/2}\mathbf{L}$ is the whitened lead-field matrix, and δ is equal to the inverse of the power signal-to-noise ratio of the whitened EEG data $\tilde{\mathbf{Z}} = \boldsymbol{\Gamma}^{-1/2}\mathbf{Z}$. In our analysis, $\delta = 1/81$. The noise covariance matrix $\boldsymbol{\Gamma}$ is

estimated based on the -300 – -100 ms baseline EEG data relative to the onset of the TMS pulses. The source-space TMS-evoked response (TER) is defined as the average of the 3-D current density across trials and represents the phase-locked response to TMS. For each subject and stimulation site, the vertex-wise TER was computed by taking the norm of the TERs of all three orientations at each vertex.

For the purposes of this paper, we examined the EEG data localized to two parcels of DLPFC that were among the parcels used for fMRI analysis: the left aMFG and left pMFG. The network TER was then obtained by averaging the vertex-wise TER across all the vertices within each network, and assessed for the following time windows by averaging within each: p30 (25-35ms), p60 (45-70ms), n100 (100-150ms), and p200 (175-225ms). For each stimulation site, participants whose average TMS-evoked response was more than 4 standard deviations away from the mean TMS-evoked response across all participants were excluded from the group analysis to ensure only high quality TMS-EEG data were analyzed.

Supplemental References

69. Drysdale AT, Grosenick L, Downar J, Dunlop K, Mansouri F, Meng Y, et al. Resting-state connectivity biomarkers define neurophysiological subtypes of depression. Nat Med. 2017;23:28–38.
70. Olshen RA, Rajaratnam B. Successive Normalization of Rectangular Arrays. Ann Stat. 2010;38:1638–1664.
71. Wu W, Keller CJ, Rogasch NC, Longwell P, Shpigel E, Rolle CE, et al. ARTIST: A fully automated artifact rejection algorithm for single-pulse TMS-EEG data. Hum Brain Mapp. 2018;39:1607–1625.
72. Hauk O. Keep it simple: a case for using classical minimum norm estimation in the analysis of EEG and MEG data. NeuroImage. 2004;21:1612–1621.
73. Gramfort A, Papadopoulo T, Olivi E, Clerc M. OpenMEEG: opensource software for quasistatic bioelectromagnetics. Biomed Eng Online. 2010;9:45.
74. Fischl B. FreeSurfer. NeuroImage. 2012;62:774–781.
75. Lin F-H, Witzel T, Ahlfors SP, Stufflebeam SM, Belliveau JW, Hämäläinen MS. Assessing and improving the spatial accuracy in MEG source localization by depth-weighted minimum-norm estimates. NeuroImage. 2006;31:160–171.

SUPPLEMENTAL TABLES 1-4:

Please see attached Excel spreadsheet

SUPPLEMENTAL FIGURES

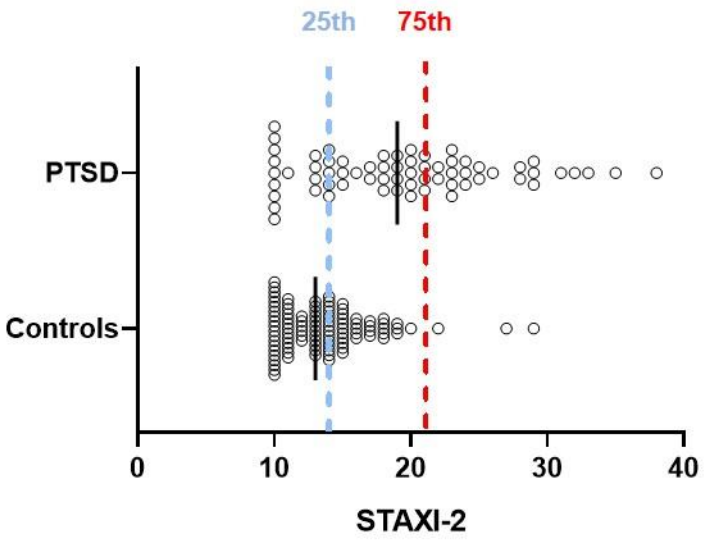

Figure S1. **Self-reported anger distribution in trauma-exposed veterans with and without PTSD**. Clinical cutoffs were used to classify participants as having high (>=75th percentile) or low (<=25th percentile) anger.

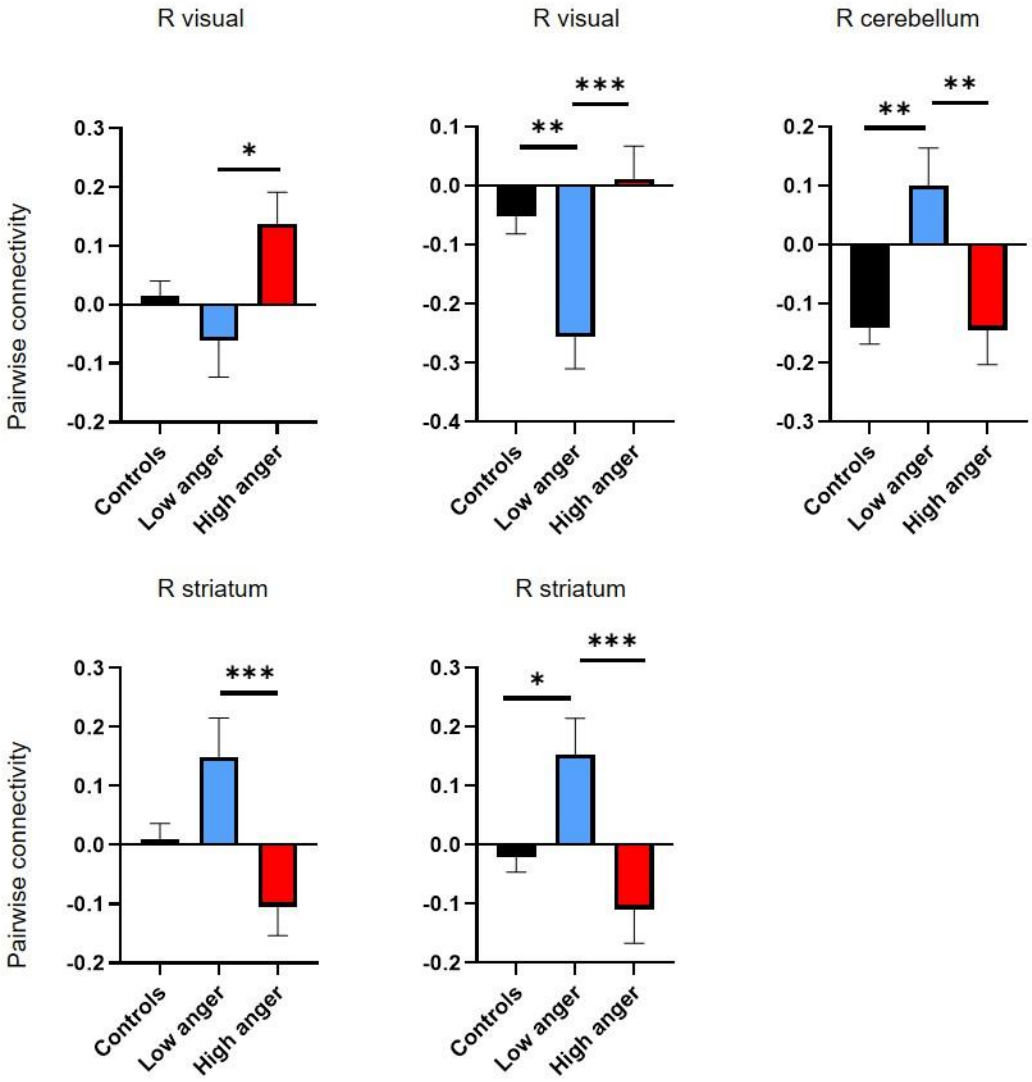

Figure S2. Pairwise connectivity from left aMFG. Posthoc pairwise comparisons were made for all five statistically-significant functional connections. *, P<0.05; **, P<0.01; ***, P<0.001

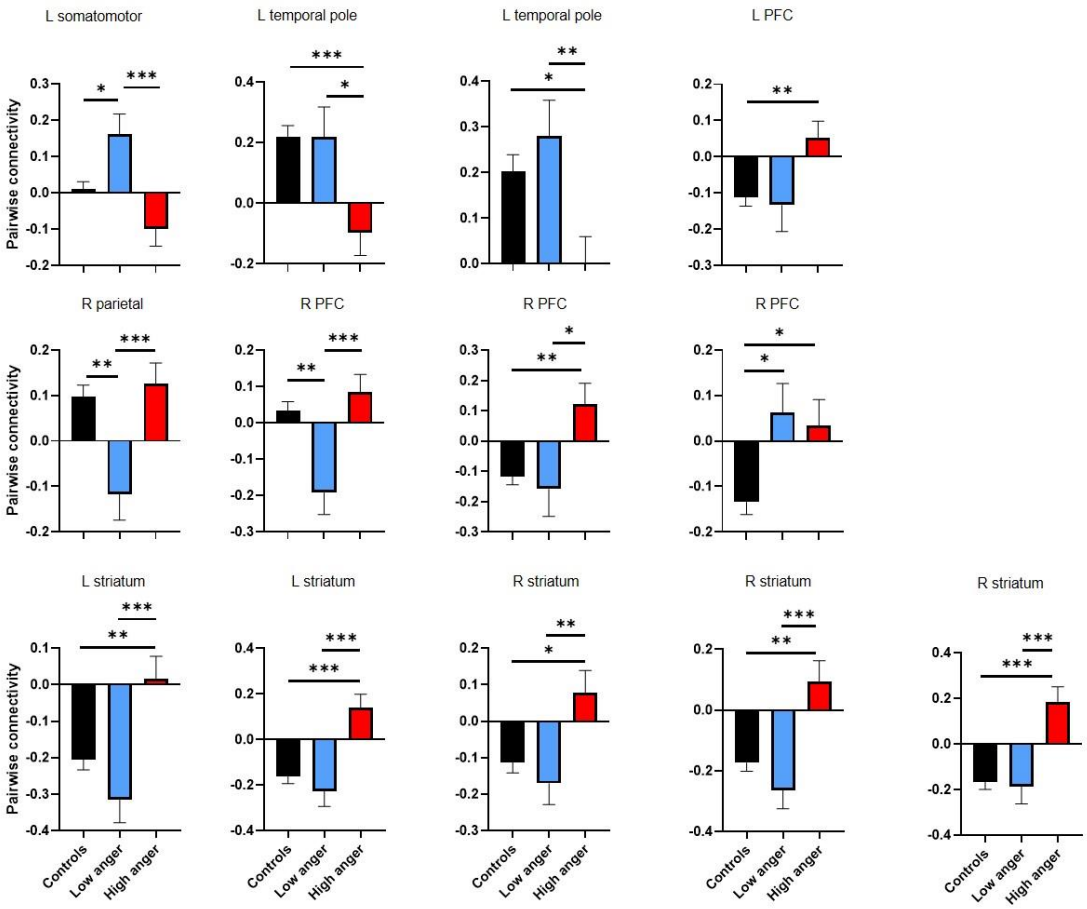

Figure S3. Pairwise connectivity from right OFC. Posthoc pairwise comparisons were made for all 13 statistically-significant functional connections. *, P<0.05; **, P<0.01; ***, P<0.001

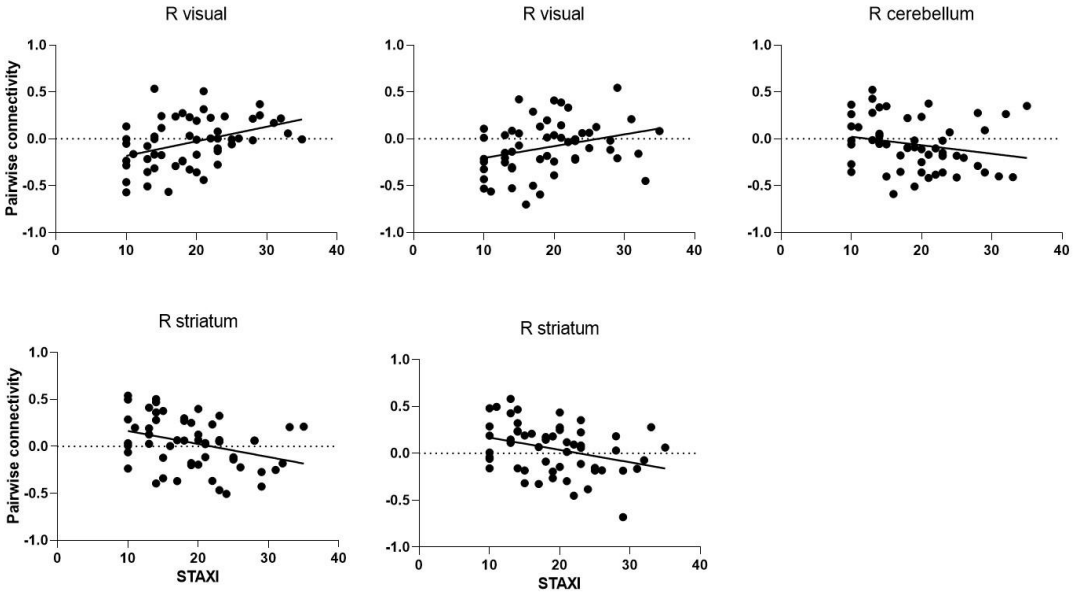

Figure S4: Pairwise connectivity from left aMFG. All five parcels with significant group differences in the GLM also showed significant correlations between anger and connectivity strength.

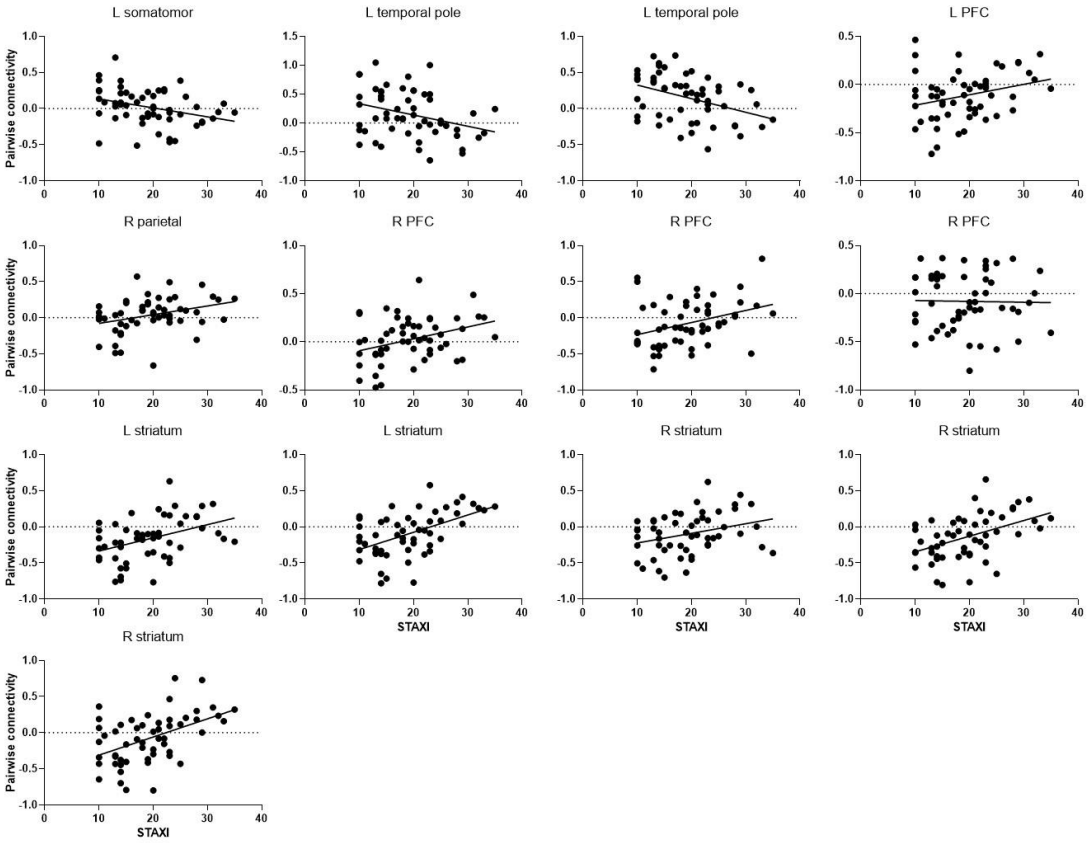

Figure S5: Pairwise connectivity from right OFC. Twelve of the 13 parcels with significant group differences in the GLM also showed significant correlations between anger and connectivity strength.

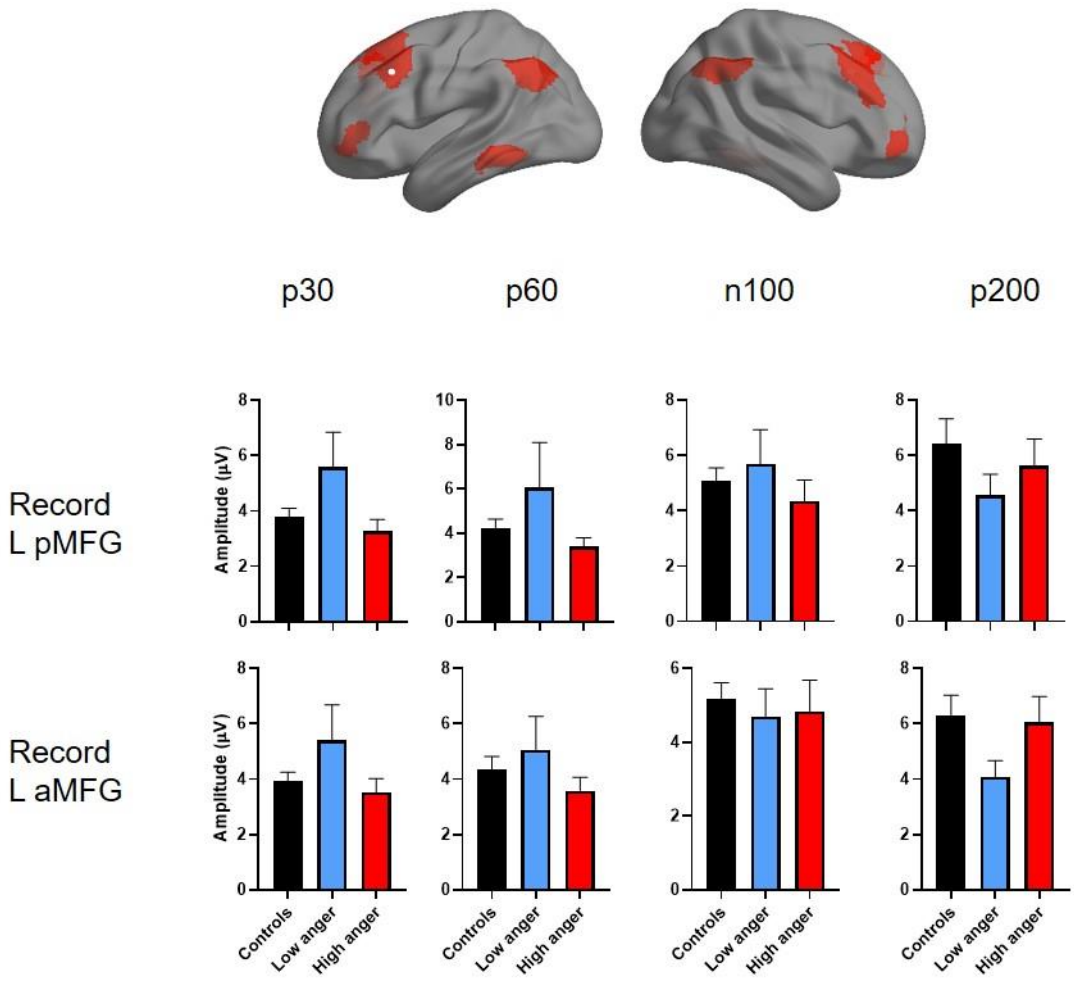

Figure S6: Spatial specificity of TMS-EEG cortical excitability findings. Top, EEG was recorded during stimulation of the left posterior middle frontal gyrus (pMFG, white sphere), a parcel of the DLPFC that neighbors the aMFG and maps onto the frontoparietal control network (red). No group differences were observed in EEG signals source-localized to the left pMFG, directly underneath the TMS coil (middle), or in EEG signals source-localized to the left aMFG (bottom).

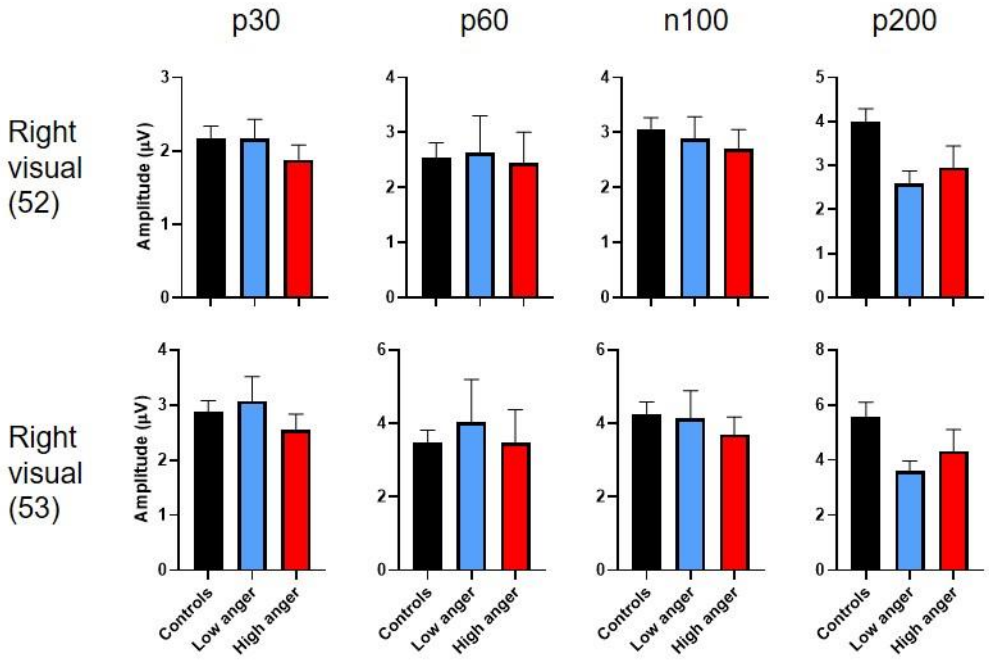

Figure S7: Spatial specificity of TMS-EEG causal connectivity findings. No group differences were observed when EEG was recorded in visual cortex during stimulation of the left posterior middle frontal gyrus (pMFG), a parcel of the DLPFC neighboring the aMFG. Top, EEG signals source-localized to right visual area 52. Bottom, EEG signals source-localized to the right visual area 53.